

# A Numerical Model of Electrical Tree Growth in Solid Insulation

**A. El-Zein, M. Talaat**

Faculty of Engineering  
Zagazig University  
Egypt

and **M. M. El Bahy**

Faculty of Engineering  
Sinai University  
Egypt

## ABSTRACT

A new model for investigating the electrical tree growth in solid insulation using a hyperbolic needle-to-plane gap is presented. The needle is embedded in the insulation medium. Classification of tree shape depends on the electric field value is presented. Then, accurate computation of the electric field is a pre-requisite for calculating electrical tree growth. The electric field distribution is obtained from Laplace's equation by treating the tree structure as an extension of the stressed electrode i.e., conducting medium. The electric field is redistributed during each growth of the electrical tree. This is achieved by using the charge simulation method. The charge at the needle surface is simulated by a group of ring charges. To determine the appropriate arrangement of simulating ring charges inside the needle, a genetic algorithm is used. A number of series finite line charge is used for simulating the charge over each branch and sub-branch during the treeing progress. The presented model for simulating electrical tree growth is a three dimensional field problem. The used needle tip radius was 3  $\mu\text{m}$  while the gap spacing varied from 0.3 to 15 mm. The results have been assessed through comparison with available analytical and experimental data.

Index Terms - Electrical tree growth, tree channel, degradation phenomena, hyperbolic needle to plane gap, charge simulation method.

## 1 INTRODUCTION

**ELECTRICAL** treeing phenomena in solid dielectric are directly related to electrical degradation of the insulating materials [1]. Polymeric insulation suffers from electrical treeing of long-term degradation when exposed to electric fields of low intensity relative to its intrinsic strength.

Breakdown in solid dielectrics has been traced to a series of partial pre-breakdown channels emanating from a region of extremely high electric stress due to imperfections present in the insulation structure, especially, due to the present of voids, impurities in the dielectric and protrusions from the inner or outside semi-conductive layer [2]. These pre-breakdown channels formed around the defect site in the dielectric structure resemble the branches of a tree. Electric charges thus penetrate into the insulation, giving rise to channels, which form the electrical tree and grow with time until breakdown [3]

There are basically three different stages in the formation of trees in the dielectrics: inception, propagation and completion [3]. In the inception phase, damage accumulates at existing defects. In the propagation phase, a branching structure originates from the defect and spreads across the dielectric. In the completion phase, the tree has bridged the gap between the electrodes [3].

The description of the geometrical characteristics of tree channel was introduced by the concept of fractal dimension to produce structures model similar to those observed in experimental studies of branching tree channels [3]. It was found that trees of low fractal dimension grew faster than trees of high fractal dimension, but trees with high fractal dimension caused great amount of damages.

In this paper, a new model for investigating the electrical tree growth in polymeric insulation is presented. This is achieved by using a hyperbolic needle-to-plane gap; the needle is embedded in the insulation medium. Tree growth mode (branch or bush type structures) was obtained by combining both of electrical and

mechanical stresses [4]. Hence, accurate computation of electric field is a pre-requisite for determining the mode and calculating the growth of electrical tree. The charge simulation method (CSM) and the method of image are used for calculating the electric field distribution. The electric field is redistributed during each step of the growth. The charge over the needle electrode is simulated by a set of ring charges. The optimum arrangement of these charges is achieved by using genetic algorithms (GAs) as a search optimization technique [5, 6]. Proposed sets of finite line charges are used for simulating the main tree stem, each inclined branch and sub-branch tree stems. The chosen needle tip radius was 3 μm and the gap spacing varied from 0.3 mm to 15 mm. The results have been assessed through comparison with available analytical and experimental data.

## 2 METHOD OF ANALYSIS

### 2.1 ELECTRICAL TREE GROWTH

#### 2.1.1 PHYSICAL APPROACH TO ELECTRICAL TREE GROWTH

The minimum electric field required to initiate a crack in the insulation medium equals to 4 MV/cm [4, 7-9]; the critical field value ( $E_c$ ).

During the growth of electrical tree, each spark filament is considered as a crack [10]. The electrostatic energy density at the crack tip ( $W_e$ )

$$W_e = \frac{1}{2} \epsilon_o \epsilon_r E^2 \quad J/m^3 \quad (1)$$

where,  $\epsilon_r$  is the relative permittivity of the dielectric medium.

At the tip of the filament there will be a very high electric field ( $E$ ). This will give rise to the mechanical stress.

The mechanical stress ( $\sigma$ ), which is induced by electric field effect, will be [10]

$$\sigma = \frac{1}{2} \epsilon_o \epsilon_r E^2 \quad J/m^3 \quad (2)$$

Then, mechanical energy density ( $W_m$ ) could be calculated from [10, 11]

$$W_m = \frac{\sigma^2}{2Y} \quad J/m^3 \quad (3)$$

where,  $Y$  is the modulus of elasticity.

The total energy ( $W$ ) will be equal to ( $W_m + W_e$ ). At breakdown,  $W_m \gg W_e$  [11]. Hence,  $W$  with respect to a unit volume will be

$$W = \left[ \frac{\sigma^2}{2Y} \right] \pi r^2 dl = \frac{\epsilon_o^2 \epsilon_r^2 \pi r^2}{8Y} E^4 dl \quad (4)$$

where,  $r$  is the crack radius with incremental length  $dl$ .

From equation (4), the total energy  $W$  is proportional to  $E^4$ . If this energy describes the critical energy  $W_c$  at a critical electric field  $E_c$ , tree initiation is reached.

$$W_c = \frac{\epsilon_o^2 \epsilon_r^2 \pi r_o^2}{8Y} E_c^4 dl_o \quad (5)$$

$$\frac{W}{W_c} = \left( \frac{E}{E_c} \right)^4 \quad (6)$$

(i.e., equal volume criterion), where,  $r_o$  is the crack radius at critical electric field  $E_c$ .

#### 2.1.2 MODES OF ELECTRICAL TREE GROWTH

For bush tree -in destroyed volume- the number of initiated cracks is very high. This number covers the entire volume.

The total number of cracks ( $N$ ) in the destroyed volume of spherical shape with radius  $R_d$  will be

$$N = \frac{\frac{4}{3} \pi R_d^3}{\frac{1}{3} \pi r_o^2 R_d} = 4 \left( \frac{R_d}{r_o} \right)^2 \quad (7)$$

The reported values of  $r_o$  and  $R_d$  are 1 μm and 10 μm, respectively [12-14], i.e.,  $R_d = 10r_o$ . Therefore,  $N$  will be equal to 400 cracks.

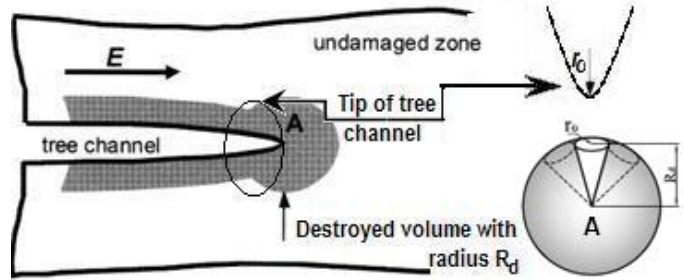


Figure 1. Microstructure of the local field around the tree channel tip; the destroyed volume with radius  $R_d$  and a tree channel with radius  $r_o$ .

In the case of two dimensions the dielectric medium breaks down mechanically when  $S/S_o = 0.6$ , where,  $S_o$  and  $S$  are the initial and the stressed spacing respectively [11]. Hence, the material is compressed by 0.4 times of initial dimension. This means that the collapsed volume equals to  $0.4^3$ .

Then, an “energy destroyed factor” will be equal to 0.064 multiplied by the  $N$  cracks, i.e.,  $n_d = 25.6$  cracks are needed to cover the destroyed volume.

Therefore, the needed critical number of cracks ( $n_c$ ), in two dimensions, for bush tree is  $n_c = \sqrt[3]{n_d} = 2.944$ . By substituting in equation (6)

$$\frac{W}{W_c} = n_c \quad (8)$$

and

$$\left( \frac{E}{E_c} \right) = \sqrt[4]{n_c} \quad (9)$$

The ratio  $E/E_c$  is equal to 1.31 for  $n_c$  equal to 2.944. Therefore,  $E/E_c < 1.31$  indicates a branch tree, and  $> 1.31$  indicates a bush tree [4].

### 2.1.3 PROPOSED STRUCTURE OF ELECTRICAL TREE GROWTH

When the electric field inside the dielectric medium reaches 4 MV/cm, the electric stress is sufficient to overcome the mechanical strength where one crack starts. However, all dielectric materials give a constant surface tension pressure of 4450 mmHg for micro-air voids when referred to ambient temperature. Its breakdown field reaches a value of 1.31 MV/cm [13], irrespective of the fact that these materials have different surface tension at its liquefied phase temperature. This value corresponds to  $(1.31/[3\epsilon_r/(2\epsilon_r+1)])$ , inside the dielectric medium. This explains the crack length of 10  $\mu\text{m}$ , which was reported by others [12-15].

From previous analysis, the proposed tree progress can be given by the following steps:

- 1- At the needle tip the electric field must reach a value of 4 MV/cm.
- 2- Under this 4 MV/cm, there is one branch crack of 1  $\mu\text{m}$  radius and 10  $\mu\text{m}$  length [12-15].
- 3- This initiated crack increases in size due to ionization at its surface, which is assumed to be a conducting medium.
- 4- A mechanical crack occurring inside dielectric material normally tapers off in radius towards its tip. This is modeled in this paper by a hyperbolic termination.
- 5- The tree is easily started from a void site and progresses towards another void. If there is no void adjacent to the needle tip, the discharge around this very high electric field needle tip will likely initiate a void. The radius of the initiated void in front of the tip will ultimately reach the tip radius value; the tree radius will then assume an equal value.
- 6- The electric tree starts from the needle tip under the electric field  $\geq 4$  MV/cm towards an air void, at which the electric field inside the void reaches the inception value ( $E_i$ ) with a crack length equal to 10  $\mu\text{m}$ .
- 7- The progress of the tree with its branches will depend on the void distribution in the medium [17]. The tree path will head for the minimum distance from the point of maximum electric field with an angle determined by the void location, Figure 2.
- 8- The void spatial distribution is produced by a computer program using the Poisson distribution, which is appropriate for this present case. It also produces random events occurring in the given region.
- 9- The present simulation calculates the electric field at each intended position in the medium considering all charges present at the surface of the needle, the main stem and all branches of the progressed tree up to this position.
- 10- At each tip the ratio of  $E/E_c$  is calculated. If this ratio is less than 1.31, it indicates one or two cracks (branch tree type). If it is greater than 1.31 it indicates more than two cracks (bush tree type).

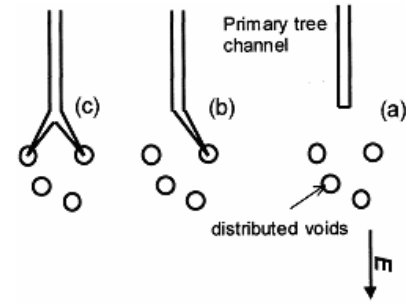


**Figure 2.** A propagating tree and its branching process. (a) Micro-voids initiate at the tree tip when the intensity of the local field ultimately builds up to some critical level; (b) the primary tree channel departs from its original straight trajectory to connect to a neighboring cavity being absorbed; (c) another neighbor cavity is absorbed by the main tree channel to form branching tree channels [17].

## 2.2 ELECTRIC FIELD CALCULATION

The progress of electrical trees in an insulating system calls at first for accurate computation of the electrostatic field. This is obtained from Laplace's equation using CSM [18]. The needle electrode is simulated by a number of ring charges. The appropriate arrangement of these ring charges is achieved by GAs.

The suggested model considers the electric field redistribution during the growth of the electrical tree. Series of vertical or inclined line charges [19, 20] are used for simulating the tree. For these inclined charges, a coordinate transformation is performed. Then, the electric field is calculated in the original coordinate system.

### 2.2.1 NEEDLE SIMULATION

Figure 3 shows a hyperbolic needle-to-plane electrode system stressed by a voltage  $V$  and embedded in solid insulation.

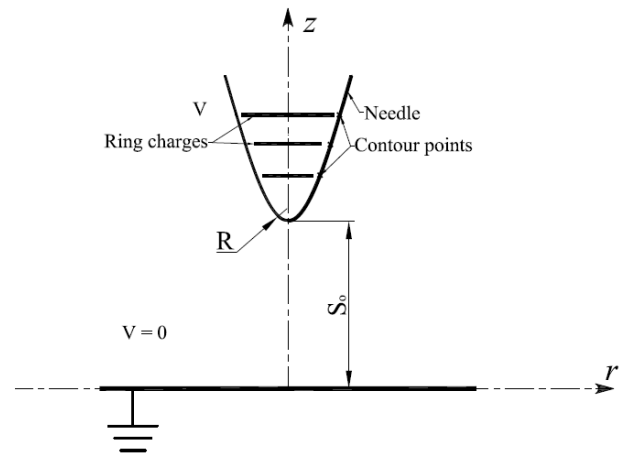


**Figure 3.** A hyperbolic needle-to-plane gap configuration.

The needle has a tip radius  $R$  and is located at spacing  $S_0$  above the grounded plane.

The shape of the needle may be described by the hyperbolic function [21]:

$$\frac{z^2}{S_0^2} - \frac{r^2}{SR} = 1 \quad (10)$$

The distributed charge on the needle surface is simulated by a set of  $n$  ring charges arranged along the needle axis. The vector of unknown charges,  $Q$  is computed from the matrix equation:

$$[P][Q] = [V] \quad (11)$$

For a given charge distribution, the potential  $\Phi$  at an arbitrary point is a summation of the potentials resulting from the individual charges,

$$\phi_i = \sum_{j=1}^n P_{ij} Q_j, \quad i = 1, 2, \dots, M \quad (12)$$

where,  $M$  and  $P_{ij}$  are the number of contour points, ( $M = n$ ) and potential coefficients, respectively.

A simple expression for the axial location of the 1<sup>st</sup> ring charge along the  $z$ -axis is presented by:

$$z_1 = S_o + f_o R \quad (13)$$

The axial location of the  $j^{\text{th}}$  ring charge along the  $z$ -axis is given by

$$z_j = z_{j-1} + (j-1)R + f_1 R, \quad j = 2, 3, \dots, n \quad (14)$$

The radius of any ring charge is determined by

$$r_j = f_2 \sqrt{R(z_j^2 - S_o^2) / S_o} \quad (15)$$

The used objective function is simply the accumulated squared error, which has the form [18]:

$$U = \sum_{i=1}^m [V - \phi_i(r, z)]^2 \quad (16)$$

The problem is now reduced to the determination of the optimum values of parameters  $f_o$ ,  $f_1$  and  $f_2$  subject to the satisfaction of the objective function given by equation (16), using GAs. In order to assess the computation accuracy, the angular deviation of the field vector at the needle surface is computed. In addition, the computed electric field, along the gap axis  $E(z)$ , is compared with the following analytical formula [21]:

$$E(z) = \frac{-2V}{a[1 - (z/a)^2] \ln[(1+w_o)/(1-w_o)]} \quad (17)$$

where,  $a = S_o \sqrt{1 + (R/S_o)}$ , and  $w_o = S_o / a$

## 2.2.2 CHARGE SIMULATION WITH TREE GROWTH

### 2.2.2.1 SIMULATION WITH MAIN TREE STEM

Initiation of a tree occurs when the electric field at the needle tip reaches  $E_c$ , under which a crack is initiated [4, 7-9]. Due to the partial discharge in the initiated crack, the medium inside it becomes conducting [12]. The field at the tip of the initiated tree becomes higher than  $E_c$ . Hence, the initiated tree tip will grow with time and form the main tree stem. The main tree stem is assumed to have a cylindrical shape having a radius  $R$  (the tip radius of the needle electrode). The main tree stem is proposed to be terminated by a hyperbolic tip having a radius  $r_o$  of the initiated tree tip, Figure 4.

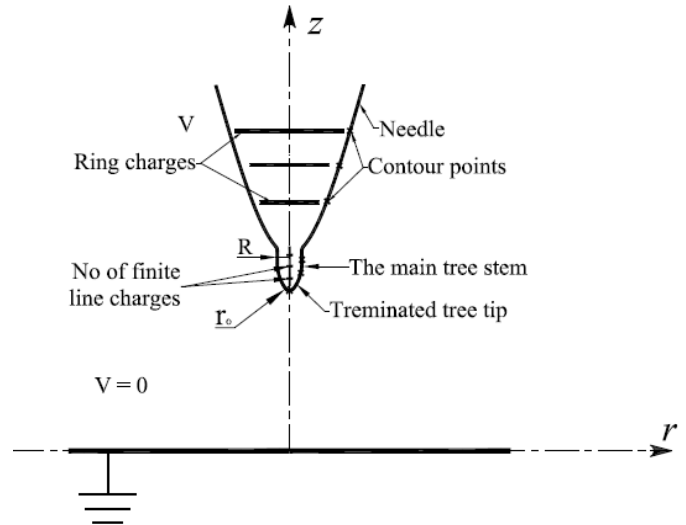


Figure 4. A hyperbolic needle with main tree stem terminated by tree tip-to-plane gap.

The main tree stem with its terminated tip is simulated by  $n_1$  finite line charges arranged along the  $z$ -axis.

Therefore, the potential at an arbitrary point is expressed by:

$$\phi_i = \sum_{j=1}^n P_{ij} Q_j + \sum_{j=n+1}^{n+n_1} P_{ij} Q_j, \quad i = 1, 2, \dots, M \quad (18)$$

where,  $M$  equals  $(n + n_1)$ .

### 2.2.2.2 SIMULATION WITH INCLINED TREE STEM

After the step taken by the main tree stem, the terminated tip is assumed to grow in an inclined direction by an angle  $\alpha_i$ , which depends on steps (7 and 8) in the proposed tree structure, having a cylindrical shape with hyperbolic terminated tip, Figure 5.

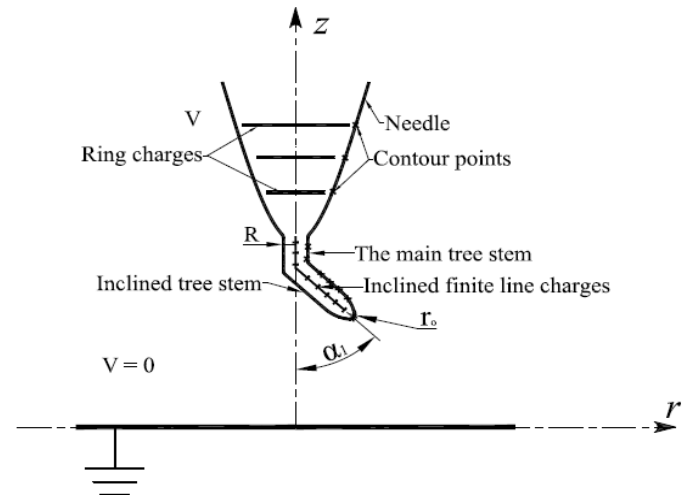


Figure 5. A hyperbolic needle with main and inclined tree stems-to-plane gap.

The inclined portion is simulated by  $n_2$  finite line charges (Appendix A). The potential at an arbitrary point is expressed by:

$$\phi_i = \sum_{j=1}^n P_{ij} Q_j + \sum_{j=n+1}^{n+n_1} P_{ij} Q_j + \sum_{j=n+n_1+1}^{n+n_1+n_2} P_{ij} Q_j, \quad i = 1, 2, \dots, M \quad (19)$$

where,  $M$  equals  $(n + n_1 + n_2)$ .

2.2.2.3 SIMULATION WITH SUB-BRANCH TREE STEM

Following the inclined tree stem, the tip of the inclined tree stem is assumed to grow in an inclined direction, at an angle  $\alpha_3$  with respect to the main z-axis, Figure 6.

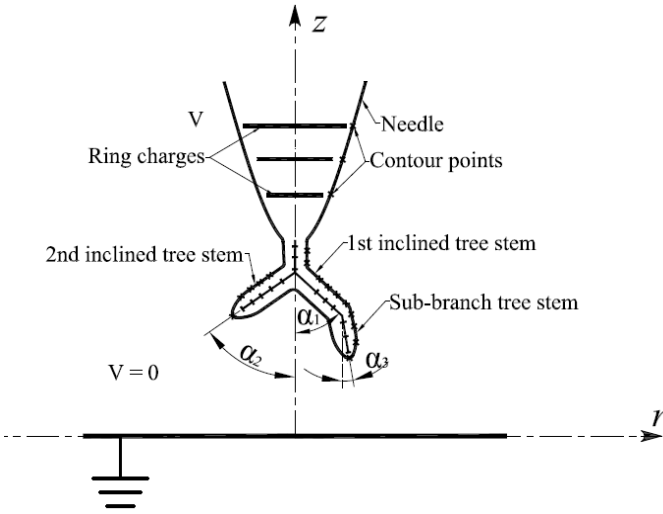


Figure 6. A hyperbolic needle with main, two inclined and one sub-branch tree stems-to-plane gap.

The sub-branch tree stem is simulated by  $n_3$  of series finite line charges. Another inclined tree stem with an angle  $\alpha_2$  may develop during this process depending on its energy with  $n_2$  finite line charges.

Then, the potential at an arbitrary point is expressed by:

$$\phi_i = \sum_{j=1}^n P_{ij} Q_j + \sum_{j=n+1}^{n+n_1} P_{ij} Q_j + \sum_{j=n+n_1+1}^{n+n_1+n_2} P_{ij} Q_j + \sum_{j=n+n_1+n_2+1}^{n+n_1+n_2+n_3} P_{ij} Q_j, i=1,2,..,M \quad (20)$$

where,  $M$  equals  $(n + n_1 + n_2 + n_3)$ .

3 RESULTS AND DISCUSSION

3.1 ELECTRICAL TREE GROWTH

Mode of electrical tree growth is determined by the number of initial cracks. This number depends on the energy level at the considered high electric field tip relative to the critical energy level at  $E_c$ .

The mode of electrical tree is determined by equation (9) as follows:

- For Branched tree
  - At one crack ( $n_c = 1$ ) i.e.,  $E/E_c = 1$
  - At two cracks ( $n_c = 2$ ) i.e.,  $E/E_c = 1.189$
- For Bush tree
  - More than two cracks ( $n_c \geq 2.944$ ) i.e.,  $E/E_c \geq 1.31$

This means that the medium at the considered site starts to collapse under three times the energy at critical field value  $E_c$ .

According to [12], the damage in a tree is defined as the ratio of (the sum of all tree channels length to the average length of the new channel) raised to the power of fractal dimension.

The range of fractal dimension varies between

- fractal dimension  $< 2$  it is considered as branched trees
- $2 < \text{fractal dimension} \leq 3$  it is considered as bush trees

Measurements on synthetic resins [12] have shown the typical dimensions of newly formed electrical tree branches to be  $\approx 10 \mu\text{m}$  long and  $1 \mu\text{m}$  radius.

The present results agree with those in [12], in which case it is possible to postulate that  $n_c$  is nearly equal to fractal dimension. This is a significant conclusion to the present work.

3.2 ELECTRIC FIELD CALCULATION

3.2.1 NEEDLE SIMULATION

In order to demonstrate the proposed approach, the used needle tip radius was  $3 \mu\text{m}$ , and the gap spacing varied from 0.3 mm to 15 mm, with  $n = 131$  ring charges. The used number of generations, population size and mutation rate in GAs [5], were 100, 10 and 0.01.

The results shown, in Figures 7, 8, 9 and 10 show that the proposed method is accurate for the examined  $G$ , where, ( $G = S_0/R$ ) range;  $G = 100$  to 5000 to cover a wide range for the simulation program.

The boundary conditions are checked over 200 times  $R$  of the needle surface and checked over 60 times of  $(R/60)$  along the tip of the needle z-axis. The simulation results are shown in Table 1.

Table 1. The simulation results of the needle.

Position	% max. absolute potential errors	max. field deviation angle (degree)
Along needle surface	0.0774	0.9504
Along needle tip	0.8598	2.7622

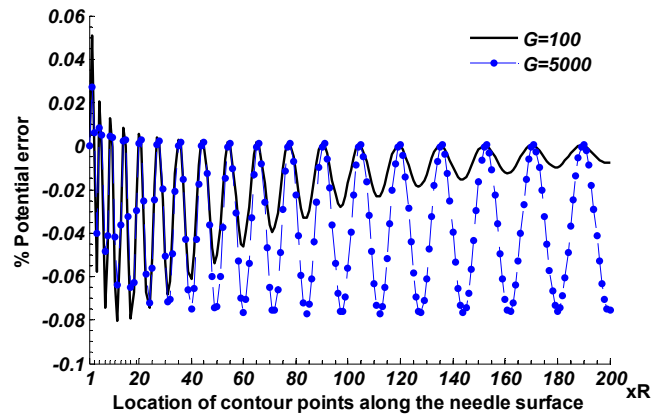


Figure 7. Variation of the per cent potential errors along the needle surface.

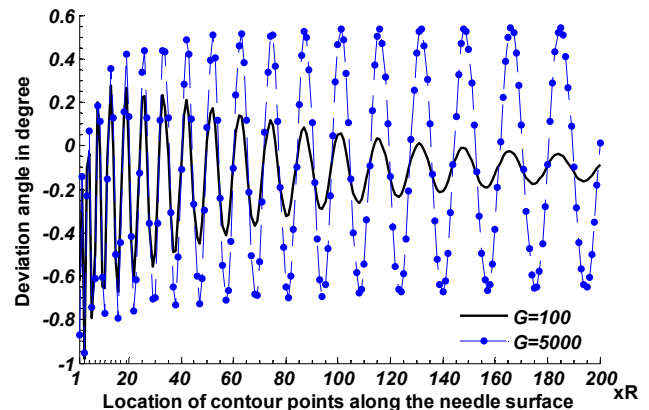


Figure 8. Variation of the deviation angle along the needle surface.

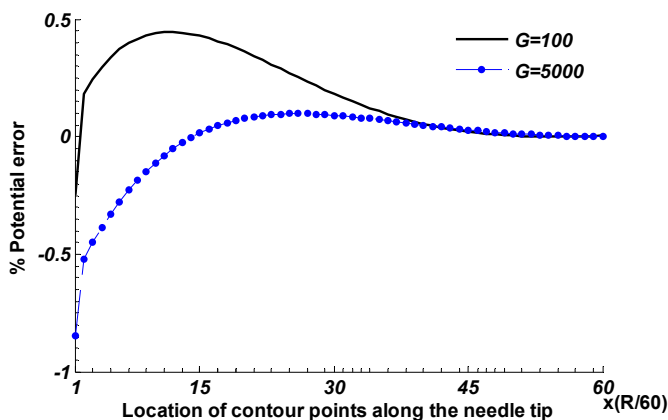


Figure 9. Variation of the per cent potential errors along the needle tip.

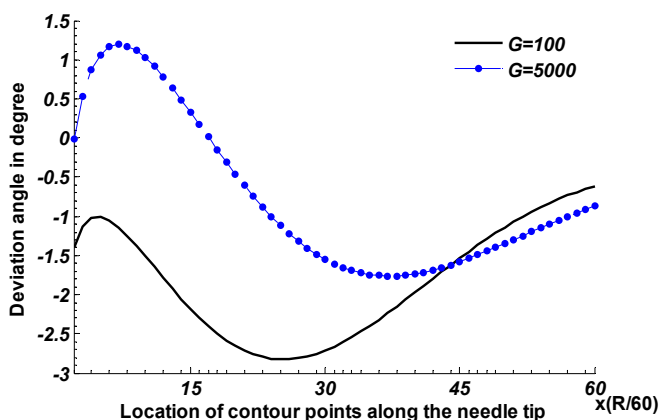


Figure 10. Variation of the deviation angle along the needle tip.

Also, the computed electric field error on the axis of the needle-to-plane gap deviates from the results of equation (17) by less than 5 %, Figure 11.

For tree simulation, the following values were used:  $R = 3 \mu\text{m}$ ,  $\epsilon_r = 2.3$  for XLPE, and  $S_o = 12 \text{ mm}$ , with  $V = 7.5 \text{ kV}$  [22].

The electric field  $E_i$  inside the dielectric medium will be  $(1.31/[3\epsilon_r/(2\epsilon_r+1)])$ , which is  $1.063 \text{ MV/cm}$  inside the dielectric medium. The axial length between the needle tip and the location, at which  $E_i$  is reached, is approximately  $10 \mu\text{m}$ , as given from Figure 12. This agrees with the  $10 \mu\text{m}$  reported in [12-15].

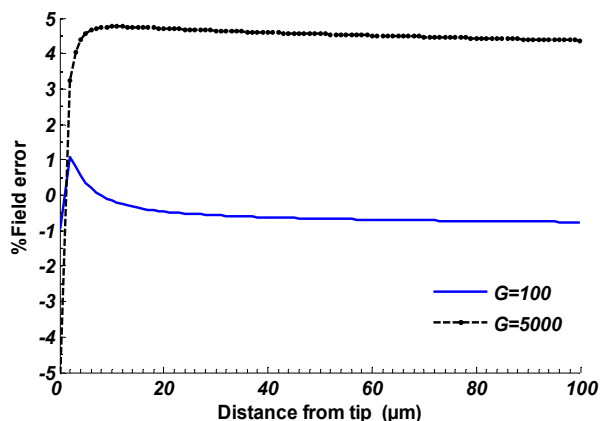


Figure 11. Per cent field error along the gap axis from analytical values.

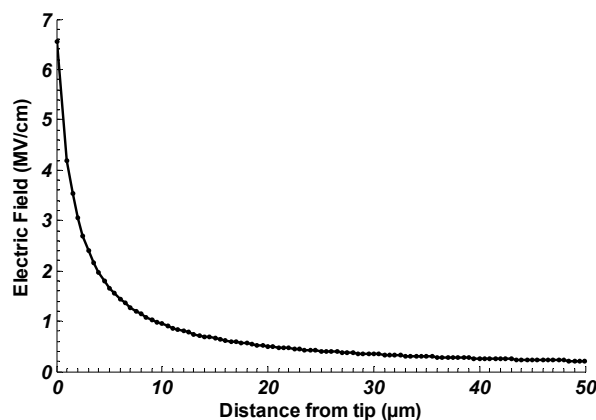


Figure 12. Electric field distributions along the gap axis using CSM.

### 3.2.2 SIMULATION WITH MAIN TREE STEM

For accurate simulation results, ( $n_1=10$ ) series finite line charges are placed equally between the main tree stem and its tip.

To check the potential error and the deviation angle over the surface of the main tree stem, 40 check points are chosen over the tip and the main stem surfaces. The simulation results are shown in Table 2.

Table 2. The Simulation Results with Main Tree Stem.

Position	% max. absolute potential errors	max. field deviation angle (degree)
Along needle surface	0.0772	1.9567
Along main tree stem surface	0.1214	3.8584
Along main tree stem tip	0.2646	2.1339

### 3.2.3 SIMULATION WITH INCLINED TREE STEM

After addition of the main tree stem to the needle electrode, the field is calculated in the direction of the nearest void, which is randomly distributed. The location of assumed void was found to exist at an angle  $\alpha_1=46$  degree from  $z$ -axis at the tree tip, which is in line with the experimental results [22-25].

The inclined tree stem is simulated by a group of finite line charges ( $n_2=10$ ) spaced equally between the inclined cylinder and its tip.

To check the potential error and the deviation angle, 30 check points are chosen over the inclined tree stem and its tip. The check points are expressed in three dimensions (Appendix B). The simulation results are shown in Table 3.

Table 3. The Simulation Results with Inclined Tree Stem.

Position	% max. absolute potential errors	max. field deviation angle (degree)
Along needle surface	0.0770	2.0608
Along main tree stem surface	0.0397	2.1950
Along inclined tree stem surface	0.1196	3.4112
Along inclined tree stem tip	0.2405	2.8958

### 3.2.4 SIMULATION WITH SUB-BRANCH TREE STEM

Based on the two inclined tree stems with angles ( $\alpha_1 = 46$  and  $\alpha_2 = 48$  degree) a sub-branch develops, which is an inclined tree stem at an angle ( $\alpha_3 = 15$  degree) with respect to



the vertical axis of the needle. The sub-branch tree stem is simulated by a number of finite line charges ( $n_3=11$ ).

To check the potential error and the deviation angle 30 check points are chosen over the sub-branch tree stem and its tip. The simulation results are shown in Table 4.

**Table 4.** The Simulation Results with Sub-Branch Tree Stem.

Position	% max. absolute potential errors	max. field deviation angle (degree)
Along needle surface	0.0852	2.2850
Along main tree stem surface	0.0837	2.7511
Along 1 <sup>st</sup> inclined tree stem surface	0.0636	1.7162
Along 2 <sup>nd</sup> inclined tree stem surface	0.1144	3.9423
Along 2 <sup>nd</sup> inclined tree stem tip	0.2079	2.8237
Along sub-branch tree stem surface	0.3878	3.9251
Along sub-branch tree stem tip	0.8701	4.1567

### 3.3 COMPARISON WITH AVAILABLE EXPERIMENTAL DATA

#### 3.3.1 TREE INITIATION COMPARISON

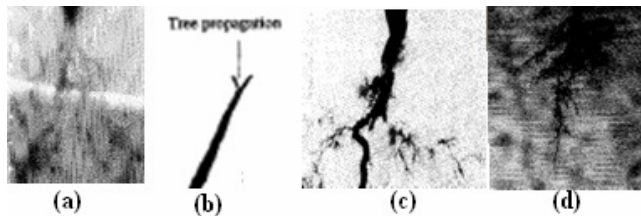
The experimental results, which shown in Figure 13, display different branch tree types.

Figure 13a,  $V = 10$  kV,  $R = 5$   $\mu$ m and  $S_o = 3$  mm after [26], in which case  $E/E_c = 1.284 < 1.31$ .

Figure 13b,  $V = 6$  kV,  $R = 3$   $\mu$ m and  $S_o = 10$  mm after [27], in which case  $E/E_c = 1.052 < 1.31$ .

Figure 13c,  $V = 10$  kV,  $R = 5$   $\mu$ m and  $S_o = 3$  mm after [28], in which case  $E/E_c = 1.284 < 1.31$ .

Figure 13d,  $V = 10$  kV,  $R = 5$   $\mu$ m and  $S_o = 5$  mm after [29], in which case  $E/E_c = 1.205 < 1.31$ .



**Figure 13.** Different branch tree types.

For all explained results the proposed model is found to be applicable in indicating the branch tree type according to the value of ( $E/E_c$ ), which is less than 1.31 for branch tree type.

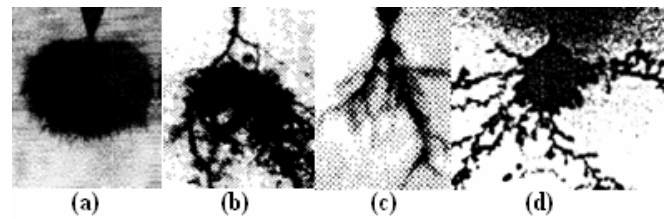
The experimental results, which shown in Figure 14, display different bush tree types.

Figure 14a,  $V = 20$  kV,  $R = 5$   $\mu$ m and  $S_o = 5$  mm after [29], in which case  $E/E_c = 2.41 > 1.31$ .

Figure 14b,  $V = 18$  kV,  $R = 3$   $\mu$ m and  $S_o = 3$  mm after [30], in which case  $E/E_c = 3.616 \gg 1.31$ .

Figure 14c,  $V = 11.31$  kV,  $R = 5$   $\mu$ m and  $S_o = 3$  mm after [25], in which case  $E/E_c = 1.45 > 1.31$ .

Figure 14d,  $V = 10$  kV,  $R = 3$   $\mu$ m and  $S_o = 12$  mm after [22], in which case  $E/E_c = 1.72 > 1.31$ .



**Figure 14.** Different bush tree types.

For all explained results the proposed model is found to be applicable in indicating the bush tree type according to the value of ( $E/E_c$ ), which is higher than 1.31 for bush tree type.

#### 3.3.2 PRESENT SIMULATION COMPARISON

Starting at a critical field of 4 MV/cm the model finds that at nearly 60% of the gap spacing a mode conversion from branch to bush takes place, which is in accordance with the corresponding value of breakdown [11]. Figure 15, shows the structure of the simulated tree. The simulated accuracy of the potential error and deviation angle did not exceed 1% and 5 degree, respectively.

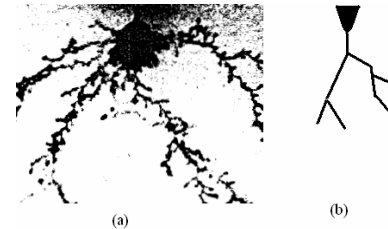


**Figure 15.** (a) experimental results using needle of tip radius equal 3 $\mu$ m, gap spacing 12mm, and applied voltage 10kV [22],  $E/E_c = 1.72$ . (b) The present simulation technique using the same data under 7.5kV,  $E/E_c = 1.29$ . Note:  $E/E_c = 1.72$  therefore tree start bush and complete branch tree.

Figure 15a, shows the experimental result using the same dimension as present simulation, yet with 10 kV, where the tree starts as a bush type,  $E/E_c = 1.72$ , and then converts into branch type tree. To ensure starting with a branch type the present simulation applies a reduced voltage is 7.5 kV.

## 4 CONCLUSIONS

1. The tree starts when the stressed tip attains a value of 4 MV/cm.
2. The path of the tree directed from the stressed tip with electric field equal or greater than 4 MV/cm toward a void location reaches the inception electric field 1.31 MV/cm inside the air void.
3. The crack length inside the dielectric medium of 10  $\mu$ m at 4 MV/cm is emphasized. This length of the tree channel predicted by the proposed method is in accordance with the previously reported experimental values.

4. The critical number of initiated cracks are  $n_c=1$ ,  $n_c=2$ , and  $n_c > 2$  for one-crack-branched tree, two-cracks-branched tree, and bush tree respectively.
5. The stressed site medium collapsed at three times the energy required by the critical field value.
6. The present results are appropriate for indicating the branch and bush types tree, depending on the value of field ratio  $E/E_c$ , which has been confirmed by comparison with many previously reported experimental results.
7. The new critical number of cracks  $n_c$  approximately equals fractal dimension reported in literature.
8. A new method is presented for simulating the tree growth in solid insulation using CSM.
9. The computed electric field error on the axis of the needle-to-plane gap deviates from the analytical solution by less than 5%.
10. The accuracy of the simulation is satisfied for the potential error, (not more than 1 %), and the field deviation angle, (not more than 5 degree) over the needle surface, the conducting channel surfaces for the main, the inclined, and the sub-branch tree stems.

## APPENDIX A

### A1. TRANSFORMATION OF COORDINATES

Each inclined finite line charge  $q$  and its image  $-q$  will be assigned to a specific Cartesian coordinate system  $(r_1, z_1)$  and  $(r_2, z_2)$ , respectively, as shown in Figure A1.1.

By transformation of coordinates, an arbitrary point  $A(r, z)$  is referred to new coordinates of line charge  $q$  and its image  $-q$ . Then, the main origin is displaced to the new origins  $(r_m, z_m)$  and  $(r_m, -z_m)$ . Hence, the new coordinates of the point  $A$  referred to the coordinate systems  $(r_1, z_1)$  and  $(r_2, z_2)$  are given as follows:

$$\begin{aligned} z_1 &= z \cos \theta - r \sin \theta \\ r_1 &= z \sin \theta + r \cos \theta \end{aligned}$$

By displacing the origin:

$$\begin{aligned} z_1 &= (z - z_m) \cos \theta - (r - r_m) \sin \theta \\ r_1 &= (z - z_m) \sin \theta + (r - r_m) \cos \theta \end{aligned}$$

Similarly,

$$\begin{aligned} z_2 &= z \cos \theta + r \sin \theta \\ r_2 &= -z \sin \theta + r \cos \theta \end{aligned}$$

By displacing the origin:

$$\begin{aligned} z_2 &= (z + z_m) \cos \theta + (r - r_m) \sin \theta \\ r_2 &= -(z + z_m) \sin \theta + (r - r_m) \cos \theta \end{aligned}$$

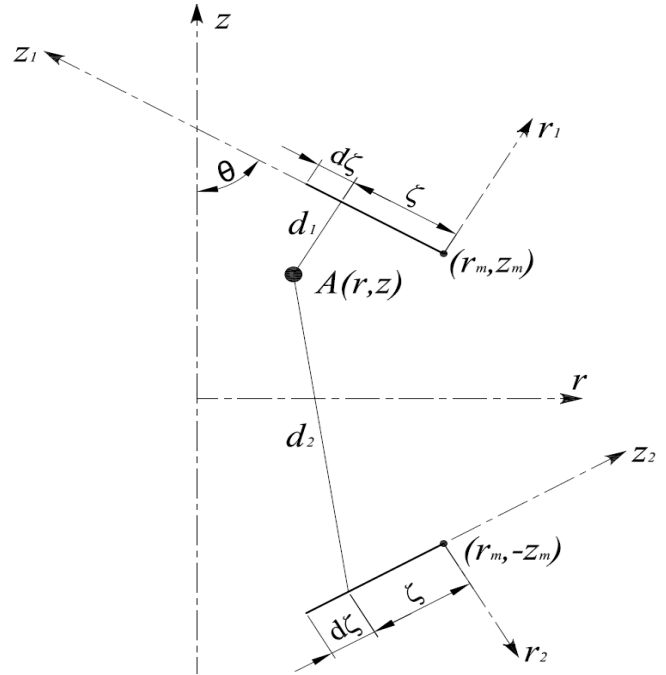


Figure A1.1 Transformation axes included the inclined line charge  $q$  and its image  $-q$

### A2. POTENTIAL CALCULATION

Each infinitesimal length  $d\zeta$  of the finite line charges  $q$  and  $-q$ , having length  $l$ , has infinitesimal charges  $dq$  and  $-dq$ , respectively.

$$dq = \frac{q}{l} \cdot d\zeta$$

After referring the coordinates of point  $A(r, z)$  to the new coordinates  $(r_1, z_1)$  and  $(r_2, z_2)$ , its potential can be calculated considering infinitesimal charges as follows:

$$d\phi = \frac{dq}{4\pi\epsilon} \left( \frac{1}{d_1} - \frac{1}{d_2} \right)$$

where,  $d_1$  and  $d_2$  are the distances between point  $A$  and the infinitesimal charges  $d\zeta$  and its image. Then,

$$\begin{aligned} d_1 &= \sqrt{(\zeta - z_1)^2 + r_1^2} \\ d_2 &= \sqrt{(\zeta + z_2)^2 + r_2^2} \end{aligned}$$

Therefore, the partial potential coefficient,  $dp$  for the infinitesimal length of charge  $d\zeta$  and its image equals

$$dp = \frac{dq}{4\pi\epsilon l} \left( \frac{1}{\sqrt{(\zeta - z_1)^2 + r_1^2}} - \frac{1}{\sqrt{(\zeta + z_2)^2 + r_2^2}} \right) d\zeta$$

Integrating along the length  $l$  of the inclined finite line charge, the potential coefficient  $p$  will be

$$p = \frac{1}{4\pi\epsilon l} \ln \left[ \frac{\left[ (l - z_1) + \sqrt{r_1^2 + (l - z_1)^2} \right] \times \left[ z_2 + \sqrt{r_2^2 + z_2^2} \right]}{\left[ (-z_1) + \sqrt{r_1^2 + z_1^2} \right] \times \left[ (l + z_2) + \sqrt{r_2^2 + (l + z_2)^2} \right]} \right]$$



Then,

$$\phi = \frac{q}{4\pi\epsilon l} \ln \left[ \frac{\left[ (l-z_1) + \sqrt{r_1^2 + (l-z_1)^2} \right] \times \left[ z_2 + \sqrt{r_2^2 + z_2^2} \right]}{\left[ (-z_1) + \sqrt{r_1^2 + z_1^2} \right] \times \left[ (l+z_2) + \sqrt{r_2^2 + (l+z_2)^2} \right]} \right]$$

### A3. FIELD CALCULATION

As well known, the electric field intensity  $E$  is the negative gradient of the potential. The differentiation of potential  $\phi$  in the coordinate systems  $(r_1, z_1)$  and  $(r_2, z_2)$  is conducted separately. Thus the components of field intensity of charge  $q$  and its image in the coordinate systems  $(r_1, z_1)$  and  $(r_2, z_2)$  are obtained, respectively.

Let:

$$\begin{aligned} \gamma_1 &= \sqrt{r_1^2 + (l-z_1)^2} & \delta_1 &= \sqrt{r_1^2 + z_1^2} \\ \gamma_2 &= \sqrt{r_2^2 + z_2^2} & \delta_2 &= \sqrt{r_2^2 + (l+z_2)^2} \end{aligned}$$

Hence, for each inclined line charge  $q$  and its image, at a contour point  $A(r, z)$ , the field intensity components  $E_{r1}, E_{z1}, E_{r2}$  and  $E_{z2}$  are

$$E_{r1} = \frac{q}{4\pi\epsilon l} \left[ \frac{l-z_1}{r_1\gamma_1} + \frac{z_1}{r\delta_1} \right]$$

$$E_{z1} = \frac{q}{4\pi\epsilon l} \left[ \frac{1}{\gamma_1} - \frac{1}{\delta_1} \right]$$

$$E_{r2} = -\frac{q}{4\pi\epsilon l} \left[ \frac{-z_2}{r_2\gamma_2} + \frac{l+z_2}{r_2\delta_2} \right]$$

$$E_{z2} = -\frac{q}{4\pi\epsilon l} \left[ \frac{1}{\gamma_2} - \frac{1}{\delta_2} \right]$$

For the superposition of the field intensity components of inclined line charge  $q$  and its image, the  $r_1, z_1$ -components as well as the  $r_2, z_2$ -components of the field intensity must be transformed back and added into the main coordinate system  $(r, z)$ . The field components, at point  $A$ , of inclined line charge  $q$  and its image in the main coordinates  $r, z$  is derived and given as follows:

$$\begin{aligned} E_z &= (E_{z1} + E_{z2})\cos\theta + (E_{r1} - E_{r2})\sin\theta \\ E_r &= (-E_{z1} + E_{z2})\sin\theta + (E_{r1} + E_{r2})\cos\theta \end{aligned}$$

## APPENDIX B

### B1. SURFACE EQUATION OF INCLINED CYLINDRICAL

Let  $\Phi_1, \Phi_2$  and  $\Phi_3$  be the angles represent the direction of cylindrical axis with respect to the main axes  $x, y, z$ , Figure B1.1.

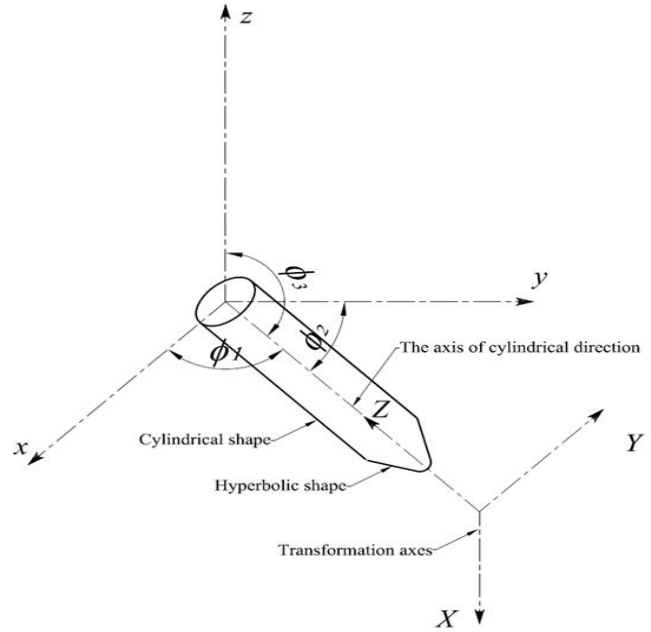


Figure B1.1 Transformation axes included the inclined cylinder and its tip.

The direction cosines of this axis are  $(\cos\phi_1, \cos\phi_2, \cos\phi_3)$ , where,  $\cos^2\phi_1 + \cos^2\phi_2 + \cos^2\phi_3 = 1$  according to [31].

Now let  $s(a, b, c)$  be the center of the sphere touching the cylinder at its base, so the equation of this sphere represented as

$$(x-a)^2 + (y-b)^2 + (z-c)^2 = r^2 \tag{B1.1}$$

And the plane containing the point  $s$  and perpendicular to the cylindrical surface may be represented by

$$\cos\phi_1(x-a) + \cos\phi_2(y-b) + \cos\phi_3(z-c) = 0.0 \tag{B1.2}$$

By taking a general point  $(\alpha, \beta, \gamma)$  on both the plane and the sphere, which represent the cylindrical surface equations (B1.1) and (B1.2) will be

$$(\alpha-a)^2 + (\beta-b)^2 + (\gamma-c)^2 = r^2 \tag{B1.3}$$

$$\cos\phi_1(\alpha-a) + \cos\phi_2(\beta-b) + \cos\phi_3(\gamma-c) = 0.0 \tag{B1.4}$$

The axes of the cylinder will be the same as the parallel direction containing the point  $(\alpha, \beta, \gamma)$

$$\frac{x-\alpha}{\cos\phi_1} = \frac{y-\beta}{\cos\phi_2} = \frac{z-\gamma}{\cos\phi_3} = t \tag{B1.5}$$

So

$$\alpha = x - t \cos\phi_1 \tag{B1.6-a}$$

$$\beta = y - t \cos\phi_2 \tag{B1.6-b}$$

$$\gamma = z - t \cos\phi_3 \tag{B1.6-c}$$

Substituting by new values of  $\alpha, \beta,$  and  $\gamma$  in equation (B1.4), to get a new value of  $t$  in terms of  $x, y,$  and  $z,$  from this

new value, the values of  $\alpha$ ,  $\beta$ , and  $\gamma$  represented by  $x$ ,  $y$ , and  $z$  can be obtained by substituting in equations (B1.6-a), (B1.6-b), and (B1.6-c)

Then, using these new values of  $\alpha$ ,  $\beta$ , and  $\gamma$  to obtain the cylindrical equation by substituting in equation (B1.3).

## B2. SURFACE EQUATION OF INCLINED HYPERBOLIC TIP

The general equation used for hyperbolic tip [31],

$$\frac{X^2}{a^2} + \frac{Y^2}{a^2} - \frac{Z^2}{b^2} = -1 \quad (B2.1)$$

At first the axes transformation are carried by considering Z-axis is the same of the cylinder  $z$ -axis but in opposite direction. Using the cosine directions of cylindrical axes ( $\cos\phi_1, \cos\phi_2, \cos\phi_3$ ), with the others axes  $X, Y$ , which must be perpendicular to the Z-axis.

$$x = Z \cos\phi_1 \quad (B2.2-a)$$

$$y = Z \cos\phi_2 \quad (B2.2-b)$$

$$z = Z \cos\phi_3 \quad (B2.2-c)$$

The dot product of  $X$  or  $Y$ -axis with  $Z$ -axis equal zero

$$\begin{bmatrix} x \\ y \\ z \end{bmatrix} = \begin{bmatrix} \cos\phi_3 & \cos\phi_1 \cos\phi_2 & \cos\phi_1 \\ 0 & -\cos^2\phi_1 - \cos^2\phi_3 & \cos\phi_2 \\ -\cos\phi_1 & \cos\phi_3 \cos\phi_2 & \cos\phi_3 \end{bmatrix} \begin{bmatrix} X \\ Y \\ Z \end{bmatrix} + \begin{bmatrix} aa \\ bb \\ cc \end{bmatrix} \quad (B2.3)$$

where, ( $aa, bb, cc$ ) represent the dimension of the center point of the transformation axes.

From equation (B2.3), we get the new values of  $X, Y, Z$  represented by  $x, y$ , and  $z$ .

Then, by substituting in equation (B2.1) the hyperbolic tree tip equation shape is obtained.

By using the point of connection between the cylindrical shape and the inclined hyperbolic shape into the equation of hyperbolic tree tip shape, the values of  $a, b$  in equation (B2.1) is obtained.

## REFERENCES

- [1] H. Kawabata, C.-S. Kim and T. Mizutani, "Partial Discharge and Light Emission in an Artificially-Simulated Narrow Tree Channel", IEEE Conf. Electr. Insul. Dielectr. Phenomena (CEIDP), pp. 19-22, 2002.
- [2] M. N. Arbab, and D. W. Auckland, "The Influence of Vibration on the Initiation of Trees in Dielectrics", IEE Proc., A, Vol. 133, pp. 618-622, 1986.
- [3] A. L. Barclay and G. C. Stevens, "Statistical and Fractal Characteristics of Simulated Electrical Tree Growth", IEE 6th Intern. Conf. Dielectric Materials, Measurements and Applications, pp. 17-20, 1992.
- [4] A. El-Zein, M. M. El Bahy, and M. Talaat, "Types of Electrical Trees in Solid Insulation under Electrical and Mechanical Energy Basis", IEEE, 12th International Middle-East Power System Conference (MEPCON), pp. 80-84, 2008.
- [5] Ryo Nishimura, K. Nishimori and N. Ishihara "Determining the Arrangement of Fictitious Charges in Charge Simulation Method using Genetic Algorithms", J. Electrostatics., Vol. 49, pp. 95-105, 2000.
- [6] M. M. Abouelsaad and M. M. El Bahy, "Accurate Field Computation of Needle-Plane Gaps using an Optimized Charge Simulation Method", IEEE Conf. Electr. Insul. Dielectr. Phenomena (CEIDP), pp. 506-509, 2000.
- [7] J. H. Mason, "Breakdown of Solid Dielectrics in Divergent Fields", Proc. IEE, Vol. 102, pp. 254-263, 1955.
- [8] L. A. Dissado and R. M. Hill, "The Statistics of Electrical Tree Inception", IEEE Trans. Dielectr. Electr. Insul, Vol. 25, pp. 660-666, 1990.
- [9] L. A. Dissado, "The Physicochemical Basis of Ageing in Polymeric Insulation", IEE Multifactor Ageing, IEE Colloquium; pp. 211-216, 1995.
- [10] J. C. Fothergill, "Filamentary Electromechanical Breakdown", IEEE Trans. Electr. Insul, Vol. 26, pp. 1124-1129, 1991.
- [11] A. El-Zein, "Effect of Extrusion Pressure on Polyethylene Cable Insulation Treeing", 9th Inter. Symposium on High Voltage Eng. (ISH) pp. 1018-1-1018-4, 1995.
- [12] J. C. Fothergill, L. A. Dissado, and P. J. J. Sweeney, "A Discharge-Avalanche Theory for the Propagation of Electrical Trees", IEEE Trans. Dielectr. Electr. Insul, Vol. 1, pp. 474-486, 1994.
- [13] A. El-Zein, "Electrically Induced Pressure under Switching Operation and Mechanical Tensile Strength as a New Measurement Tools of Cable Aging", IEEE International Symposium on Electrical Insulating, pp. 155-158, 1996.
- [14] E. J. McMahan, "The Chemistry of Corona Degradation of Organic Insulating Materials in High Voltage Fields and Under Mechanical Strain", IEEE Trans. Electr. Insul, Vol. 3, pp. 3-10, 1968.
- [15] N. Hozumi, T. Okamoto, and H. Fukagawa, "TEM Observation of Electrical Tree Paths and Micro-Structures in Polyethylene", IEEE International Symposium on Electrical Insulating, Boston, MA, USA, pp.331-334, 1998.
- [16] M.A. Brown, J. V. Champion, S. J. Dodd, and P. Mudge, "An Investigation of Partial Discharge Energy Dissipation and Electrical Tree Growth in an Epoxy Resin", IEEE Intern. Conf. Solid Dielectrics, (ICSD), Vol. 1, Toulouse, France, pp. 288-291, 2004.
- [17] H.-Z. Ding and B. R. Varlow, "Thermodynamic Model for Electrical Tree Propagation Kinetics in Combined Electrical and Mechanical Stresses", IEEE Trans. Dielectr. Electr. Insul, Vol. 12, pp. 81-89, 2005.
- [18] N. H. Malik, "A Review of the Charge Simulation Method and its Applications", IEEE Trans. Electr. Insul, Vol. 24, pp. 3-20, 1989.
- [19] D. Utmischi, "Charge Substitution Method for Three-Dimensional High Voltage Fields", 3rd Inter. Symposium on High Voltage Eng. (ISH), Milan, Italy, paper number 11.01, 1979.
- [20] M. M. El-Bahy, M. Abouelsaad, N. Abdel-Gawad and M. Badawi, "Onset Voltage of Negative Corona on Stranded Conductors", J. Phys. D: Appl. Phys., Vol. 40, pp. 3094-3101, 2007.
- [21] W. L. Lama and C. F. Gallo, "Systematic Study of the Electrical Characteristics of the "Trichel" Current Pulses from Negative Needle to Plane Coronas", J. Appl. Phys. Vol.45, pp. 103-113, 1974.
- [22] K. Wu, H. Xie, Y. Suzuoki, and T. Mizutani, "The Effect of Conductivity Distribution in Tree Channel on PD Behavior in Electrical Tree", IEEE Intern. Sympos. Electr. Insulating Materials, Japan, pp. 701-704, 1998.
- [23] A. El-Zein, "Analysis of Water Treeing in Solid Insulated Cables", IEEE International Symposium on Electrical Insulating, Arlington, Virginia, USA, pp.113-116, Vol. 1, 1998.
- [24] E. Wantanabe, M. Yoshizawa, and T. Moriya, "Ultrasonic Visualization of Electrical trees", IEEE Conf. Electr. Insul. Dielectr. Phenomena (CEIDP), pp.431-436, 1994.
- [25] L. Ziyu, L. Rongsheng, W. Huiming and L. Wenbin "Space Charges and Initiation of Electrical Trees", IEEE Trans. Electr. Insul. Vol. 24, pp. 83-89, 1989.
- [26] R. Bozzo, F. Guastavino and G. C. Montanari, "Electrical Tree Tests: Probabilistic Inference and Insulating Material Evaluation", IEEE Trans. Dielectr. Electr. Insul. Vol. 5, pp. 734-740, 1998.
- [27] H. Kaneiwa, Y. Suzuoki and T. Mizutani, "Partial Discharge Characteristics and Tree Inception in Artificial Simulated Tree Channels", IEEE Trans. Dielectr. Electr. Insul. Vol. 7, pp. 843-848, 2000.
- [28] D. W. Auckland, J. M. Cooper and B. R. Varlow, "Factors Affecting Electrical Tree Testing", IEE Proc.-A, Vol. 139, pp. 9-13, 1992.

- [29] E. David, J. L. Parpal and J.-P. Crine, "Influence of Internal Mechanical Stress and Strain on Electrical Performance of Polyethylene", IEEE Trans. Dielectr. Electr. Insul, Vol. 3, pp. 248-257, 1996.
- [30] S. H. Kang, K. J. Lim, H. Park and M. N. Kim, "Correlation between Partial Discharges and Electrical Treeing in Low Density Polyethylene Blended with Organic Additives", IEEE 4th Inter. Conf. Properties and Applications of Dielectric Materials (ICPADM); pp. 409-411, 1994.
- [31] J. L. Merian and L. G. Kraige, *Engineering Mechanics Statics*, 5th ed., Vol.1, Von-Hoffman Press, USA, pp. 5-8, 2002.



**A. El-Zein** (professor) was born in El-Dakahlia, Egypt in 1948. He received the B.Sc. and M.Sc. degrees from the Faculty of Engineering, Cairo University, Egypt in 1971, and 1977 respectively, and the Ph.D. degree from Ain-Shams University in 1985. Now he is the Head of the Electrical Power and Machines Department, Faculty of Engineering, Zagazig University. The research interest covers different types of high voltage insulation, breakdown of dielectric materials (gasses, liquids and solids).



**M. M. El Bahy** (professor) was born in El-Kalyobia, Egypt in 1955. He received the B.Sc. degree from the Faculty of Engineering, Shoubra, Zagazig University, Egypt in 1978, the M.Sc. and Ph.D. degrees from the Faculty of Engineering, Cairo University, Egypt in 1983 and 1991, respectively. Now he is professor in the Faculty of Engineering, Sinai University. The research interest covers different types of Corona studies, breakdown of dielectric materials, and digital calculation of electric fields.



**M. Talaat** (Ph.D. Student) was born in El-Sharkia, Egypt in 1979. He received the B.Sc. and M.Sc. degrees from the Faculty of Engineering, Zagazig University, Egypt in 2000, and 2005, respectively, and now he is an Assistant Lecturer at Zagazig University, Egypt. He has many published papers in IEEE conferences (CEIDP 2008, MEPCON 2003, 2005, 2008), ISH 2009. The research interest covers different types of high voltage insulation, Computer programs using simulation models.